

# Controlling Size-Induced Phase Transformations Using Chemically Designed Nanolaminates\*\*

Matt Beekman,\* Sabrina Disch, Sergei Rouvimov, Deepa Kasinathan, Klaus Koepernik, Helge Rosner, Paul Zschack, Wolfgang S. Neumann, and David C. Johnson\*

Since the initial observation of melting-point reduction with size for gold nanoparticles,<sup>[1]</sup> the relative stability of crystalline phases has also been demonstrated to be size-dependent in a number of technologically important materials, including CdSe<sup>[2]</sup> and CdS,<sup>[3]</sup> Al<sub>2</sub>O<sub>3</sub>,<sup>[4]</sup> and various other metal oxides<sup>[5]</sup> and chalcogenides.<sup>[6]</sup> As the surface free energy contribution to the total free energy becomes increasingly important as the size of a system is decreased, a crystalline phase with lower surface free energy may be favored with respect to the thermodynamically stable bulk phase when the crystallite size is smaller than a critical value in one or more dimensions.<sup>[2–7]</sup> The role of size as an effective thermodynamic parameter is of fundamental importance, but also provides a mechanism for controlling the crystal structure of a material, and therefore its properties.

Although precise control of surface chemistry and nanocrystal size in well-defined material systems is prerequisite to understanding and controlling size-induced phenomena, it nevertheless remains challenging to achieve. Although impressive progress has been made in the preparation of ensembles of inorganic nanocrystals with relatively narrow size distributions,<sup>[8]</sup> the preparation of nanocrystal ensembles of completely uniform size that can be tuned with atomic precision would constitute a significant synthetic advance, in particular for the application of size-dependent structural and physical properties. Using a combination of experimental and computational techniques, we demonstrate herein that chemically designed nanolaminates, consisting of an intergrowth of chemically and structurally distinct components, comprise a class of materials in which this level of control can be

achieved for one crystallographic direction. As a consequence of the ability to precisely control size, the crystal structure of the components can be tuned via a size-induced transformation. In contrast to epitaxial superlattices, which experience structural distortions due to strain induced by epitaxial interfaces,<sup>[9]</sup> the intergrowths reported on in the present work lack an epitaxial relationship between the components. This structural independence of the constituents allows the effect of size on crystal structure to be delineated from strain effects.

It was recently discovered<sup>[10]</sup> that [(MSe)<sub>1+δ</sub>][TSe<sub>2</sub>]<sub>n</sub> intergrowths can be prepared by the modulated elemental reactants (MER) synthetic route.<sup>[11]</sup> Here M = {Pb, Sn, Bi, Ce}, T is an early transition metal, and the integers *m* and *n* denote the number of consecutive layers of the respective components in the repeating unit of the intergrowth (Figure 1). The value of *δ* reflects the difference in the in-plane atomic packing density for the independent component structures in the intergrowth (hereafter we use the designation [MSe]<sub>m</sub>[TSe<sub>2</sub>]<sub>n</sub> for convenience).

We chose to explore the SnSe–MoSe<sub>2</sub> system for several reasons. Along with the prospect of developing novel nanocrystalline SnSe materials for optoelectronic and photovoltaic applications,<sup>[12]</sup> bulk crystalline SnSe undergoes a second-order (continuous) structural phase transition from α-SnSe (GeS structure type) to β-SnSe (ThI structure type) as the temperature is increased.<sup>[13]</sup> As the parent compounds SnSe and MoSe<sub>2</sub> (Figure 1a and b) are both layered semiconductors, significant charge transfer between the components in the intergrowth is not expected. A stable interface exists

[\*] Prof. M. Beekman  
Department of Natural Sciences  
Oregon Institute of Technology  
Klamath Falls, OR 97601 (USA)  
E-mail: matt.beekman@oit.edu

Dr. S. Disch,<sup>[†]</sup> Prof. Dr. W. S. Neumann, Prof. D. C. Johnson  
Department of Chemistry, University of Oregon  
Eugene, OR 97403 (USA)  
E-mail: davej@uoregon.edu

Prof. S. Rouvimov  
Department of Electrical Engineering  
University of Notre Dame  
Notre Dame, IN 46556 (USA)


Dr. D. Kasinathan, Dr. H. Rosner  
Max Planck Institute for Chemical Physics of Solids  
01187 Dresden (Germany)

Dr. K. Koepernik  
IFW Dresden  
P.O. Box 270116, 01171 Dresden (Germany)

Dr. P. Zschack  
Advanced Photon Source, Argonne National Lab  
Argonne, IL 60439 (USA)

[†] Present address: Institut Laue-Langevin  
38042 Grenoble (France)

[\*\*] This work was supported by the NSF through CCI grant CHE-1102637, and grant MRI 0923577 provided equipment used in this investigation. M.B. acknowledges support from the NSF under grant DMR 0907049. S.R. and W.S.N. acknowledge support from ONR Award No. N000141110193. Use of the Advanced Photon Source, an Office of Science User Facility operated for the U.S. Department of Energy (DOE) Office of Science by Argonne National Laboratory, was supported by the U.S. DOE under Contract No. DE-AC02-06CH11357. The authors thank J. Karapetrova and D. Robinson for their assistance in collection of the synchrotron X-ray diffraction data, and C. Heideman and D. Moore for useful discussions.

 Supporting information for this article is available on the WWW under <http://dx.doi.org/10.1002/anie.201305377>.

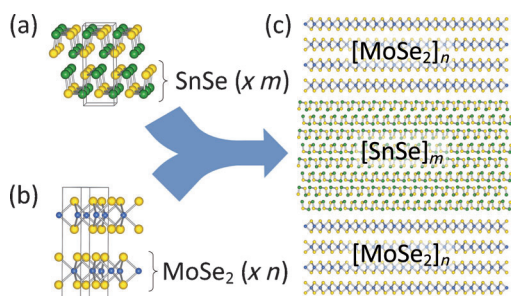


**Figure 1.** Crystal structures of the (bulk) binary compounds a) SnSe and b) MoSe<sub>2</sub>. Conceptually, the structural unit of each component used to describe the SnSe-MoSe<sub>2</sub> intergrowth is a single layer (indicated by brackets), corresponding in each case to one-half the crystallographic unit cell of the bulk compound. c) Illustration of a segment of a SnSe-MoSe<sub>2</sub> intergrowth; the layer sequence repeats along the intergrowth direction. (The intralayer rotational disorder of the MoSe<sub>2</sub> component is not reflected in this illustration.)

between SnSe and MoSe<sub>2</sub>, allowing high-quality intergrowths to be prepared,<sup>[10c]</sup> while the available data indicate a lack of epitaxy and minimal interfacial strain between the components in these materials.<sup>[7,10]</sup> Based on these considerations, we expected we could control the size of SnSe nanocrystals by trapping them between MoSe<sub>2</sub> layers in an intergrowth (Figure 1c). By controlling the effective nanocrystal size by the intergrowth profile, we hypothesized that the crystal structure of the SnSe component might be continuously tuned by a size-induced structural transformation.

[SnSe]<sub>m</sub>[MoSe<sub>2</sub>]<sub>n</sub> intergrowth thin films were formed by annealing thin film precursors prepared by physical vapor deposition as previously reported;<sup>[10c]</sup> further details can be found in the Supporting Information. Upon identification of the optimal precursor deposition conditions and post-deposition annealing (723 K for 30 min under an oxygen-free atmosphere), high quality SnSe-MoSe<sub>2</sub> intergrowths were obtained. Extensive diffraction maxima (Figure 2a; Support-

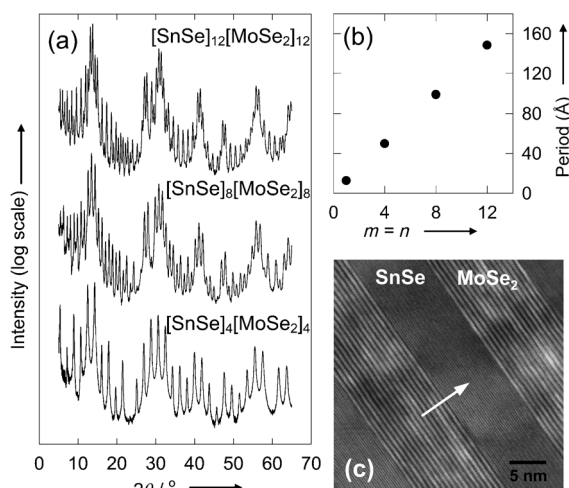


**Figure 2.** a) Specular X-ray diffraction patterns (log scale; spectra stacked vertically) collected from [SnSe]<sub>m</sub>[MoSe<sub>2</sub>]<sub>n</sub> intergrowths with  $m=n=4, 8$ , and  $12$ . b) Intergrowth period as a function of  $m=n$ . c) HAADF STEM image from an intergrowth with  $m=15$ . The arrow indicates the substrate normal ( $c$ -axis of the intergrowth).

ing Information, Figure S1, log scale intensity) observed from specular X-ray diffraction (XRD) are collectively indexed as  $(00l)$  reflections using a single  $c$ -axis parameter (overall period of the intergrowth) that increases regularly as the number of layers of both components ( $m=n$  in this case) is increased (Figure 2b). The formation of precisely layered SnSe-MoSe<sub>2</sub> periodic superstructures along the substrate normal is further confirmed by high-angle annular dark field scanning transmission electron microscopy (HAADF-STEM, Z-contrast) imaging (Figure 2c). By controlling the composition profile in the deposited thin film precursor, the individual layer thickness of each constituent can be systematically and independently controlled, and a broad range of SnSe thicknesses with  $1 < m < 30$  have been synthesized. These values correspond to significantly larger component thicknesses than previously achieved in [MSe]<sub>m</sub>[TSe<sub>2</sub>]<sub>n</sub> intergrowths.<sup>[7,10,14]</sup>

High-resolution transmission electron microscopy (HRTEM) imaging (Figure 3a) reveals significant turbostratic (rotational) disorder throughout the thickness of the MoSe<sub>2</sub> component, shown by different orientations that are visible progressing from layer to layer. Such observations have also been made in previous characterization of MER-prepared TX<sub>2</sub>-based materials.<sup>[7,10,15]</sup> In contrast to this, we observe a propensity for SnSe to form coherent nanocrystalline domains, where the crystallite size along the  $c$ -axis of the intergrowth is constrained by the thickness of the SnSe layer rather than turbostratic disorder. The different behavior of SnSe (no intralayer turbostratic disorder) and MoSe<sub>2</sub> (exten-

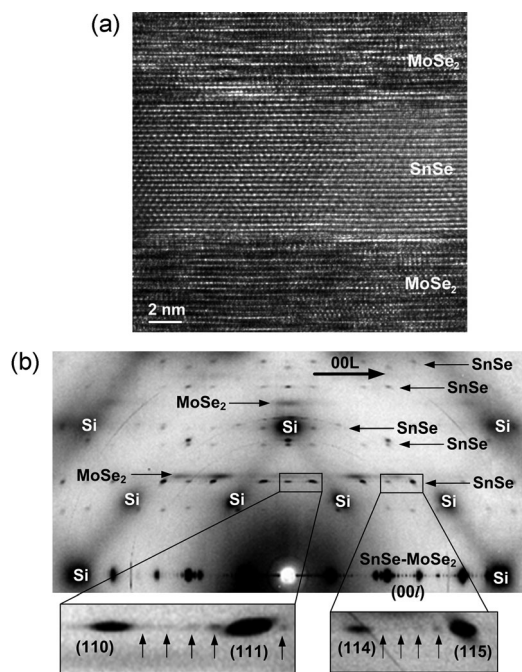


**Figure 3.** a) HRTEM image of the same SnSe-MoSe<sub>2</sub> intergrowth shown in Figure 2c. b) Synchrotron XRD data collected from a [SnSe]<sub>12</sub>[MoSe<sub>2</sub>]<sub>12</sub> specimen using an area detector. Reflections originating from SnSe and MoSe<sub>2</sub> are labeled. Zoomed regions show secondary maxima owing to the finite size of the SnSe nanocrystals along the intergrowth direction. (The diamond-like pattern of broad reflections and faint narrow rings originate from the silicon substrate and sample holder, respectively.)

sive intralayer turbostratic disorder) reflects the sequential templated nucleation of MoSe<sub>2</sub> layers<sup>[15]</sup> and is understandable considering the presumably small energy difference between the various stacking polytypes reported for transition-metal dichalcogenides.<sup>[16]</sup> We also observe extensive interlayer turbostratic (rotational) disorder between the SnSe layers that are separated by MoSe<sub>2</sub>.

The interpretation of the HRTEM data is supported by high-energy synchrotron XRD, which provides access to a significant volume of reciprocal space. Data collected using an area detector (Figure 3b) reveal three important features originating from the film: 1) a series of (00 $l$ ) diffraction peaks originating from the SnSe-MoSe<sub>2</sub> intergrowth (analogous to the specular diffraction data of Figure 2a); 2) a series of reflections that can be indexed to an orthorhombic unit cell for SnSe; and 3) a series of comparatively broad, diffuse reflections that can be indexed to MoSe<sub>2</sub>. As opposed to mixed reflections corresponding to a [SnSe]<sub>12</sub>[MoSe<sub>2</sub>]<sub>12</sub> periodic superstructure, only ( $hkl$ ) reflections originating from the individual SnSe and MoSe<sub>2</sub> components are observed in any scattering direction other than  $L$  (Figure 3b), which is consistent with the lack of registry between the components.<sup>[10]</sup> As  $m$  is increased, the SnSe reflections become significantly sharper along  $L$  owing to decreased finite size broadening of the reflections,<sup>[17]</sup> which is further indication that the nanocrystallite size of SnSe along the  $c$  direction is indeed limited by the component thickness,  $m$  (see the Supporting Information for further details).

Closer examination of the diffracted intensity originating from the SnSe component reveals weak secondary maxima located at regularly spaced positions along  $L$  between the main SnSe ( $hkl$ ) reflections (Figure 3b), which is attributed to incomplete destructive interference of X-rays scattered from the SnSe nanocrystals of finite (and uniform) size. Although the theory of diffraction from very small crystals predicts such features (see the Supporting Information for further discussion),<sup>[17]</sup> they are rarely observed experimentally in nanocrystalline systems.<sup>[7,17,18]</sup> The HRTEM and synchrotron XRD data collectively support the conclusion that our SnSe-MoSe<sub>2</sub> intergrowths comprise an ensemble of nanocrystalline SnSe domains that have precise crystallographic alignment and uniform size along the  $c$ -direction that is limited to be equal to the thickness of the SnSe component.

The size-induced structural transformation in SnSe was revealed by collecting synchrotron XRD data as a function of  $m$ . Under standard conditions, the thermodynamically stable  $\alpha$ -SnSe phase crystallizes with the orthorhombic GeS-type structure (Figure 1a), characterized by intralayer Sn–Se covalent bonds and weaker interlayer interactions, with Sn and Se each in (3+2) coordination.<sup>[13a]</sup> As  $T$  is increased, the basal plane lattice parameters of bulk  $\alpha$ -SnSe continuously approach a common value up to the transition temperature 807 K (Figure 4a, open symbols), above which the more symmetric  $\beta$ -SnSe phase (ThI-type structure) is stable.<sup>[13a]</sup> Turning to the structure of our [SnSe] <sub>$m$</sub>  nanocrystals, the basal plane lattice parameters<sup>[19]</sup> (Figure 4a, solid symbols) continuously approach a common value as the axial size of the nanocrystal ( $m$ ) is reduced. These data corroborate previous observations from more conventional nanoparticle systems

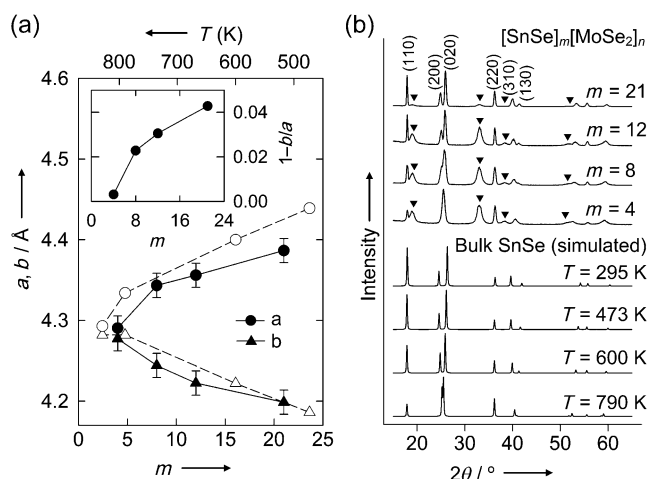


**Figure 4.** a) Basal plane lattice parameters (at 294 K) for the SnSe component as a function of  $m$  (solid symbols), as well as basal plane lattice parameters for bulk SnSe<sup>[13a]</sup> as a function of temperature (open symbols, top axis). Inset: Fractional difference between  $a$  and  $b$  as a function of  $m$ . b) Top: Experimental in-plane XRD patterns collected from [SnSe] <sub>$m$</sub> [MoSe<sub>2</sub>] <sub>$n$</sub>  intergrowths as a function of  $m$  (spectra stacked vertically). ( $hk0$ ) reflections of SnSe are indexed, those of MoSe<sub>2</sub> indicated by  $\blacktriangledown$ . Bottom: Simulated ( $hk0$ ) XRD patterns for bulk  $\alpha$ -SnSe as a function of temperature (based on crystallographic data from Ref. [13a]).

that the reduction of size can have a similar effect on structural stability as an increase in the temperature.<sup>[2,4–6]</sup>

Synchrotron XRD patterns collected using an in-plane geometry (scattering vector in the basal plane of the components; Figure 4b) only contain ( $hk0$ ) reflections that are again readily indexed<sup>[19]</sup> using orthorhombic and hexagonal basal plane lattice parameters for SnSe and MoSe<sub>2</sub>, respectively. These data are also representative of a two-dimensional nanocrystalline powder of SnSe and MoSe<sub>2</sub>, both having near perfect axial alignment parallel to the substrate normal and random orientations within the basal plane. For comparison (Figure 4b, bottom), ( $hk0$ ) powder XRD patterns as a function of  $T$  were simulated<sup>[21b]</sup> using the crystallographic data for bulk  $\alpha$ -SnSe reported by Chattopadhyay et al.<sup>[13a]</sup> Systematic trends in the reflection intensities and positions as  $m$  is decreased (or  $T$  is increased) originate from continuous shifts in the basal plane lattice parameters and atomic positions ( $x$  and  $y$ ) of Sn and Se that accompany the continuous  $\alpha \rightarrow \beta$  transition, ultimately resulting in a change in coordination from 3+2 in  $\alpha$ -SnSe to 4+1 in  $\beta$ -SnSe and a corresponding modification of the Sn–Se bonding.<sup>[13]</sup>

Calculations of optimized geometries by density functional theory (DFT) using a periodic slab model for SnSe ( $m = 2, 4, 6, 8$ , and bulk SnSe) confirmed the nature of the structural transformation. In agreement with the experimental results, the basal plane lattice parameters are observed to approach a common value as the thickness of the slab is reduced (Supporting Information, Figure S3), providing confirmation that the transformation is indeed size-induced and not driven by the interaction with the MoSe<sub>2</sub> constituent in spite of the composite nature of these materials. As DFT is a ground-state theory and thus corresponds to  $T = 0$  K, the ratio  $a:b$  for the DFT predicted structures is consistently



higher than the corresponding experimental ratio for each  $m$  (from DFT, the predicted bulk value is effectively reached at a thickness of  $m = 8$ ). This is expected, because the structural transformation is not only size-dependent but also temperature-dependent<sup>[13a]</sup> (Figure 4a), therefore the ratio  $a:b$  for a given  $m$  is expected to decrease as temperature is increased. Taken together, the experimental and computational results validate the concept of a size-dependent phase diagram for the second-order  $\alpha$ -SnSe  $\rightarrow$   $\beta$ -SnSe phase transition, as similarly proposed for size-dependent first-order transitions in other materials.<sup>[2–6]</sup>

To conclude,  $[\text{MX}]_m[\text{TX}_2]_n$ -type nanolaminates comprise material systems in which the physical extent of the nanocrystalline components can be “dimensionally constrained” with atomic precision by merely changing the thickness of the layers, allowing the crystal structure of one or more of the components to be controlled by size-induced structural transformations. The non-epitaxial nature of these intergrowths allows size effects to be delineated from strain effects that are commonly encountered in epitaxial superlattices. We believe these observations have several important implications. Considering that the detailed understanding of how structure depends on size in crystalline nanoparticles remains relatively undeveloped, the ability to extract details of the atomic structure from ordered arrays of nanocrystals is an important feature of these systems. In principle, intergrowth compounds provide a platform for materials design, in which computational methods can help identify the structures and compositions that may be of interest. Lastly, the use of size and/or surface chemistry as an energetic parameter to tune the crystal structure of a material offers a potentially powerful approach for tuning functionality. An intriguing possibility afforded by intergrowth structures is the prospect of influencing the surface free energy of one component by the choice of the second component, which may offer an additional avenue for controlling crystal structure in conjunction with size.<sup>[3]</sup> Given the broad compositional space that is possible in such intergrowth materials,<sup>[7,10,14,20]</sup> we expect that these implications can be readily explored.

## Experimental Section

$[\text{SnSe}]_m[\text{MoSe}_2]_n$  thin films were prepared by physical vapor deposition using the modulated elemental reactants synthetic approach.<sup>[11]</sup> Specular X-ray diffraction and reflectivity data were collected (Bruker D8 Discover) using  $\text{CuK}\alpha$  radiation and parallel beam optics. Synchrotron X-ray diffraction data were collected at the Advanced Photon Source at beamlines 33-BM-C and 6-ID-D. Structure analysis by means of high-resolution TEM and STEM was carried out at 300 kV (FEI Titan 80-300 equipped with an imaging lens Cs aberration corrector and a high-angle annular dark-field detector). Creation of Figures 1 and 4 was aided by the software described in Ref. [21a,b], respectively. Further experimental and computational details may be found in the Supporting Information.

Received: June 22, 2013

Published online: October 16, 2013

**Keywords:** chalcogenides · layered compounds · metastable compounds · nanostructures · phase transitions

- [1] P. Buffat, J.-P. Borel, *Phys. Rev. A* **1976**, *13*, 2287.
- [2] a) S. H. Tolbert, A. P. Alivisatos, *Science* **1994**, *265*, 373; b) C.-C. Chen, A. B. Herhold, C. S. Johnson, A. P. Alivisatos, *Science* **1997**, *276*, 398; c) A. S. Karakoti, S. Sanghavi, P. Nachimuthu, P. Yang, S. Thevuthasan, *J. Phys. Chem. Lett.* **2011**, *2*, 2925.
- [3] A. Nag, A. Hazarika, K. V. Shanavas, S. M. Sharma, I. Dasgupta, D. D. Sarma, *J. Phys. Chem. Lett.* **2011**, *2*, 706.
- [4] a) J. M. McHale, A. Navrotsky, A. J. Perrotta, *J. Phys. Chem. B* **1997**, *101*, 603; b) J. M. McHale, A. Auroux, A. J. Perrotta, A. Navrotsky, *Science* **1997**, *277*, 788.
- [5] a) P. Ayyub, V. R. Palkar, S. Chattopadhyay, M. Multani, *Phys. Rev. B* **1995**, *51*, 6135; b) A. A. Gribb, J. F. Banfield, *Am. Mineral.* **1997**, *82*, 717; c) H. Zhang, J. F. Banfield, *J. Mater. Chem.* **1998**, *8*, 2073; d) G. Baldinozzi, D. Simeone, D. Gosset, M. Dutheil, *Phys. Rev. Lett.* **2003**, *90*, 216103.
- [6] J. B. Rivest, L.-K. Fong, P. K. Jain, M. F. Toney, P. A. Alivisatos, *J. Phys. Chem. Lett.* **2011**, *2*, 2402.
- [7] M. D. Anderson, C. L. Heideman, Q. Lin, M. Smeller, R. Kykyneshi, A. A. Herzog, I. M. Anderson, D. A. Keszler, P. Zschack, D. C. Johnson, *Angew. Chem.* **2013**, *125*, 2036; *Angew. Chem. Int. Ed.* **2013**, *52*, 1982.
- [8] C. B. Murray, C. R. Kagan, M. G. Bawendi, *Annu. Rev. Mater. Sci.* **2000**, *30*, 545; B. L. Cushing, V. L. Kolesnichenko, C. J. O’Conner, *Chem. Rev.* **2004**, *104*, 3893.
- [9] Z. Hiroi, *Philos. Mag. B* **1990**, *61*, 895.
- [10] a) C. L. Heideman, N. Nguyen, J. Hanni, Q. Y. Lin, S. Duncombe, D. C. Johnson, P. Zschack, *J. Solid State Chem.* **2008**, *181*, 1701; b) Q. Y. Lin, M. Smeller, C. L. Heideman, P. Zschack, M. Koyano, M. D. Anderson, R. Kykyneshi, D. A. Keszler, I. M. Anderson, D. C. Johnson, *Chem. Mater.* **2010**, *22*, 1002; c) M. Beekman, G. Cogburn, C. Heideman, S. Rouvimov, P. Zschack, W. Neumann, *J. Electron. Mater.* **2012**, *41*, 1476.
- [11] D. C. Johnson, *Curr. Opin. Solid State Mater. Sci.* **1998**, *3*, 159.
- [12] a) M. A. Franzman, C. W. Schlenker, M. E. Thompson, R. L. Brutchey, *J. Am. Chem. Soc.* **2010**, *132*, 4060; b) W. J. Baumgardner, J. J. Choi, Y.-F. Lim, T. Hanrath, *J. Am. Chem. Soc.* **2010**, *132*, 9519; c) S. Liu, X. Guo, M. Li, W.-H. Zhang, X. Liu, C. Li, *Angew. Chem.* **2011**, *123*, 12256; *Angew. Chem. Int. Ed.* **2011**, *50*, 12050; d) L. Li, Z. Chen, Y. Hu, X. Wang, T. Zhang, W. Chen, Q. Wang, *J. Am. Chem. Soc.* **2013**, *135*, 1213.
- [13] a) T. Chattopadhyay, J. Pannetier, H. G. von Schnerring, *J. Phys. Chem. Solids* **1986**, *47*, 879; b) W. Tremel, R. Hoffmann, *Inorg. Chem.* **1987**, *26*, 118.
- [14] G. A. Wieggers, *Prog. Solid State Chem.* **1996**, *24*, 1.
- [15] R. A. Atkins, D. B. Moore, D. C. Johnson, *Chem. Mater.* **2013**, *25*, 1744.
- [16] a) J. A. Wilson, A. D. Yoffe, *Adv. Phys.* **1969**, *18*, 193; b) J. A. Wilson, F. J. Di Salvo, S. Mahajan, *Adv. Phys.* **1975**, *24*, 117.
- [17] A. Guinier, *X-ray Diffraction in Crystals, Imperfect Crystals, and Amorphous Bodies*, W. H. FREEMAN, San Francisco, **1963**.
- [18] P. Croce, G. Devant, M. Gandais, A. Marraud, *Acta Crystallogr.* **1962**, *15*, 424.
- [19] For the  $c$ -axis of SnSe to coincide with the intergrowth direction (substrate normal) and  $a$  and  $b$  in the basal plane of the layers, we describe the structure of SnSe using space group setting  $Pcmn$ , which differs from  $Pbnm$  used in Ref. [13a] ( $c$ -parameter in the basal plane).
- [20] a) R. Atkins, J. Wilson, P. Zschack, C. Grosse, W. Neumann, D. C. Johnson, *Chem. Mater.* **2012**, *24*, 4594; b) D. B. Moore, M. Beekman, S. Disch, P. Zschack, I. Häusler, W. Neumann, D. C. Johnson, *Chem. Mater.* **2013**, *25*, 2404; c) C. L. Heideman, S. Tepfer, Q. Lin, R. Rostek, P. Zschack, M. D. Anderson, I. M. Anderson, D. C. Johnson, *J. Am. Chem. Soc.* **2013**, *135*, 11055.
- [21] a) T. C. Ozawa, S. J. Kang, *J. Appl. Crystallogr.* **2004**, *37*, 679; b) W. Kraus, G. Nolze, *J. Appl. Crystallogr.* **1996**, *29*, 301.